Biomaterials Science

ROYAL SOCIETY OF CHEMISTRY

PAPER

View Article Online
View Journal

Cite this: DOI: 10.1039/d1bm00174d

Hepatic differentiation of human embryonic stem cells by coupling substrate stiffness and microtopography†

Chunhua Luo,‡[a] Dongyuan Lü,‡[a,b] Lu Zheng,[a,b] Fan Zhang,[a,b] Xiao Zhang,[a,b] Shouqin Lü,[a,b] Chen Zhang,[a] Xiaohua Jia,[c] Xinyu Shu,[a,b] Peiwen Li,[a] Zhan Li[a] and Mian Long *[a,b]

Mechanical or physical cues are associated with the growth and differentiation of embryonic stem cells (ESCs). While the substrate stiffness or topography independently affects the differentiation of ESCs, their cooperative regulation on lineage-specific differentiation remains largely unknown. Here, four topographical configurations on stiff or soft polyacrylamide hydrogel were combined to direct hepatic differentiation of human H1 cells *via* a four-stage protocol, and the coupled impacts of stiffness and topography were quantified at distinct stages. Data indicated that the substrate stiffness is dominant in stemness maintenance on stiff gel and hepatic differentiation on soft gel while substrate topography assists the differentiation of hepatocyte-like cells in positive correlation with the circularity of H1 clones initially formed on the substrate. The differentiated cells exhibited liver-specific functions such as maintaining the capacities of CYP450 metabolism, glycogen synthesis, ICG engulfment, and repairing liver injury in CCl_4-treated mice. These results implied that the coupling of substrate stiffness and topography, combined with the biochemical signals, is favorable to improve the efficiency and functionality of hepatic differentiation of human ESCs.

Received 30th January 2021,
Accepted 29th March 2021

DOI: 10.1039/d1bm00174d

rsc.li/biomaterials-science

Introduction

Human embryonic stem cells (hESCs) are pluripotent stem cells derived from the inner cell mass of blastocysts and have a prolonged undifferentiated proliferation potential *in vitro* when cultured under appropriate conditions. Stemness (*i.e.*, pluripotency) and differentiation of hESCs are regulated by the extracellular microenvironment, such as mechanical or physical cues around cells, soluble molecules, and cell–cell interactions.[1] Directing hepatic differentiation of hESCs is not only crucial in understanding hepatic organogenesis *in vivo*, but also able to provide a sufficient source of cells for repairing liver injury or damage for therapeutic purposes. Hepatic differentiation of ESCs usually undergoes multiple stages including definitive endoderm, hepatic progenitor cells, and mature hepatocytes.[2] Various transcription factors, growth factors, cytokines, glucocorticoids, and exogenous factors are known to be key biochemical regulators,[3,4] in the presence or absence of serum[5,6] or in a two- (2D) or three-dimensional (3D) cell culture.[7] However, the mechanisms of mechanical or physical cues in directing hepatic differentiation are largely unclear.

Mechanical forces play critical roles in embryonic development. For instance, dynein-driven cilia generate leftward nodal flow at the node, governing the specification of the left–right axis in early embryogenesis.[8] During embryonic implantation, a continuous cyclic extension enforces the blastocyst escape from the zona pellucida and defines the embryonic polarity.[9,10] Contractile forces are generated to pull the margin cells during zebrafish epiboly in gastrulation.[11] These *in vivo* mechanical cues can be deciphered by various *in vitro* approaches when placing ESCs onto substrate. Moreover, the mechanical features of the extracellular matrix (ECM) or substrate itself also affects the biological functions of ESCs in addition to the exerted shear, tension or contraction. hESCs exhibit different definitive endodermal differentiation on soft and stiff substrates, and high endodermal gene expression is

[a]*Center for Biomechanics and Bioengineering, Key Laboratory of Microgravity (National Microgravity Laboratory) and Beijing Key Laboratory of Engineered Construction and Mechanobiology, Institute of Mechanics, Chinese Academy of Sciences, Beijing 100190, China. E-mail: mlong@imech.ac.cn; Fax: +86-10-82514131; Tel: +86-10-82514131*

[b]*School of Engineering Science, University of Chinese Academy of Sciences, Beijing 100049, China*

[c]*CAS Key Laboratory of Molecular Imaging, Institute of Automation, Chinese Academy of Sciences, Beijing 100190, China*

†Electronic supplementary information (ESI) available. See DOI: 10.1039/d1bm00174d

‡These authors contributed equally to this work.

found on moderately stiff substrates.[12] Meanwhile, different substrate topographies and geometries alter the stemness of ESCs on polyacrylamide (PA) hydrogel[13] and manipulate their mesodermal, endodermal, or ectodermal differentiation on fibrils.[14] Thus, it is critical to elucidate the impacts of the *in vivo* mechanical or physical microenvironment on differentiation of ESCs, especially when considering their organ-specific complexity.

Complicated mechanical or physical cues existing in early embryogenesis are also present in the liver. In the elementary building blocks of the liver lobule, multiple types of hepatic cells reside inside liver sinusoids and are exposed to blood flow on the top of the liver endothelium and to interstitial flow underneath the endothelium.[15,16] All the cells and extracellular matrix proteins form distinct configurations, *i.e.*, discontinuous endothelial lining, tabular structured hepatocytes, or discretely distributed stellate cells, which, together with the supporting basal membrane appearing in liver fibrosis or cirrhosis, present complicated topographies inside the sinusoids.[17] Meanwhile, progressive liver fibrosis or cirrhosis aggravates the stiffness of hepatic tissues up to ten-fold higher, resulting from the augmented deposits of collagen I and other ECM proteins inside the Disse space.[18] Thus, elucidating the roles of these mechanical or physical cues is meaningful not only for the directed endodermal differentiation in embryonic development but also for the functional implementation of differentiated hepatocytes. To date, however, little is known about how substrate stiffness and substrate topography separately or cooperatively modulate hepatic differentiation of ESCs.

Previously, we tested the coupled impacts of substrate stiffness and topography on maintaining mouse ESC stemness and directing rat bone mesenchymal stem cell (MSC) differentiation.[13,19] Here, we extended this well-defined approach to understand the mechanical regulation of hepatic differentiation of hESCs. Typical two stiffnesses and four topographies were proposed to characterize the *in vivo* anatomical structures of liver sinusoids and mimic the pathophysiological progress of liver fibrosis. An *in situ* four-stage continuous differentiation protocol was established to induce hESC differentiation from pluripotent cells through definitive endodermal lineage and precursor hepatocytes to hepatocyte-like cells (HLCs) on PA gel. Cell growth, differentiation, and liver-specific functions were tested at the protein and gene levels or in mice with liver injury and the coupled impacts of substrate stiffness and topography were studied.

Experimental

Ethics statement

All experiments involving the use of human embryonic stem cell line H1 and animal research and care procedures were conducted in accordance with the guidelines of the Institutional Animal and Medicine Ethical Committee (IAMEC). All the protocols were approved by the IAMEC at the Institute of Mechanics, Chinese Academy of Sciences.

Fabrication of PA hydrogel substrates

Topographical substrates were fabricated using PA hydrogels *via* a previously described soft-contact lithography technique.[13,19] Briefly, 40% acrylamide (Amresco, Washington, USA) and 2% bis-acrylamide (Sigma-Aldrich, St Louis, MO, USA) were added into water to form a solution with a constant concentration of 10% acrylamide and two varied concentrations of 0.03 and 0.30% bis-acrylamide. After adding 1/200 (v/v) of 10% curing agent ammonium persulfate (Amresco) and 1/2000 (v/v) accelerating agent *N*,*N*,*N*′,*N*′-tetramethylethylenediamine (Amresco) to the mixture, the mask designed for the desired planar or topographical configurations was suspended for 30 min at room temperature (RT). The PA hydrogel was solidified, removed, and then incubated in deionized water overnight. After adding 0.2 mg ml^{-1} cross-linking agent sulfo-SANPAH (Thermo Fisher Scientific, Waltham, MA, USA) in an appropriate volume, the mixture was irradiated with ultraviolet light for 20 min. The planar hydrogel was cut into rectangular bands to test its Young's modulus using a self-weighing assay, yielding 6.1 (soft) and 46.7 (stiff) kPa at the respective bis-acrylamide concentrations.[13,19] The topographical hydrogel was then prepared in disc-like shape (20 mm in diameter and 0.1 cm in thickness) with three configurations: grooved (ridge width/ditch width = 15/5 μm), square pillar (side-length/inter-pillar gap size = 10/10 μm), or hexagonal (ridge width/side-length = 5/15 μm) with the same depth of 5 μm. A planar hydrogel with the same diameter and thickness was used as the control. 650 μl of 200 μg ml^{-1} collagen I was cross-linked stably onto the hydrogel surface before seeding the cells.[12]

Cell culture and hepatic differentiation on varied substrates

Human embryonic stem cells (H1) were authorized for use by the WiCell Research Institute (Madison, WI, USA) and were maintained on a matrigel-coated (Corning, New York, NY, USA) polystyrene dish in mTeSR 1 medium (Stem Cell Technologies, Vancouver, BC, Canada) at 37 °C under 5% CO_2. The medium was exchanged daily, and routine cell passage was performed *via* a Dispase (Stem Cell Technologies) digestion method for 8 min. The undifferentiated colonies were collected using a StemPro EZPassage Disposable Stem Cell Passaging Tool (Invitrogen, Waltham, MA, USA), followed by gently pipetting them into small aggregates and dispensing the aggregates onto various PA hydrogel surfaces.

To direct H1 cell differentiation into HLCs, the cells were first cultured on planar or topographical hydrogel for three days in feeder cell (the human skin fibroblast from ATCC) conditioned medium,[13] followed by a 1-day culture in RPMI medium (Gibco, Waltham, MA, USA) supplemented with 100 ng ml^{-1} activin A (Roche, Basel, Switzerland) and 5% FBS (Gibco) and a 2-day culture in the above medium supplemented with 0.5 mM sodium butyrate (Sigma-Aldrich). A subsequent 7-day culture was done in knock-out DMEM (Invitrogen) supplemented with 0.1% DMSO (Sigma-Aldrich), 1% non-essential amino acids (Invitrogen), 20% KnockOutTM serum replacement (Invitrogen), 0.1 mM β-mercaptoethanol

(Invitrogen), and 1 mM glutamine (Invitrogen), followed by a final 2-day culture in L15 medium (Gibco) supplemented with 10 ng ml^{-1} HGF (R&D, Minneapolis, MN, USA), 20 ng ml^{-1} human oncostatin M (R&D), 10% FBS, 1 mM insulin (Sigma-Aldrich), 10 μM hydrocortisone 21-hemisuccinate (Sigma-Aldrich) and 2 mM glutamine (Invitrogen) (Fig. 1a). This protocol defined the four sequential stages of hepatic differentiation of H1 cells on a PA hydrogel substrate, that is, stemness maintenance (STEM), definitive endodermal lineage (DE), precursor hepatocytes (Pre-H), and hepatocyte-like cells or HLCs (M-H). In some cases, a matrigel-coated polystyrene dish was used to maintain H1 cell culture in the same time courses for comparisons.

Optical or scanning electron microscopy (SEM)

At the STEM stage, H1 cells were cultured on either PA hydrogel or matrigel-coated dishes for three days and then imaged using an inverted microscope (Olympus IX71, Tokyo, Japan) at a magnification of 4× or 10×. For each topographical substrate, the number of H1 colonies was counted, and the projected area, aspect ratio between the long and short axes, and circularity (defined as $4\pi \times$ area/perimeter2) of the colonies were measured for quantitative comparisons. At the DE, Pre-H or M-H stage, the respective induction medium as indicated above was added and the optical images were acquired.

A morphological study was also conducted using SEM imaging of H1 cells and differentiated cells on PA hydrogel or matrigel-coated dishes. The samples were fixed at a given time point, prepared with a conventional protocol,[20] and examined using an SEM device (FEI Quanta 200, FEI, USA). Sample preparation and image acquisition on four topographical PA gels (planar, groove, square pillar, and hexagonal) with two stiffnesses alone were also performed in the absence of H1 cells, using the same protocol as that used for the cells on PA gel.

Immunofluorescence staining and confocal microscopy

Cells cultured on PA hydrogel or a matrigel-coated dish were rinsed with PBS (Corning) at pH 7.2, fixed for 15 min in 4% paraformaldehyde (Amresco), and permeabilized with 0.4% Triton X-100 (Sigma-Aldrich) for 10 min. After blocking non-specific epitopes using 1% BSA (Sigma-Aldrich) at 37 °C for 1 h, the collected cells were stained with primary monoclonal antibodies (mAbs) at 37 °C for 1 h, incubated at 4 °C overnight, and rinsed five to seven times with PBS. An adequate amount of the

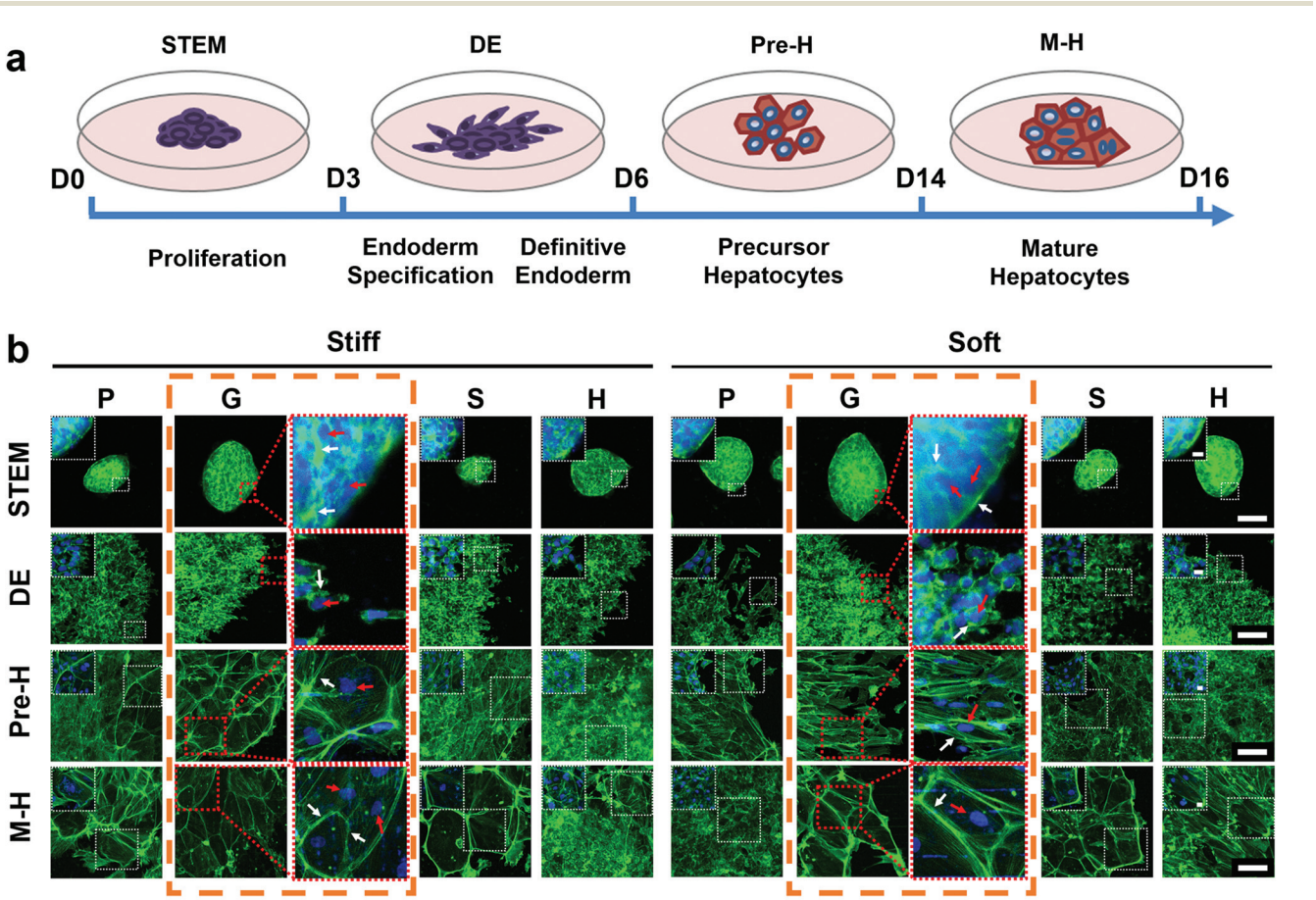

Fig. 1 Growing H1 cells on PA hydrogels at distinct stages. (a) Protocols illustrating a modified four-stage strategy of hepatic differentiation. (b) Immunostaining of actin (green) and nuclei (blue) for H1 cells on topographical PA hydrogels pre-coated with 200 μg ml^{-1} collagen I in planar (P), grooved (G), square pillar (S), or hexagonal (H) configuration on stiff (46.7 kPa) or soft (6.1 kPa) substrates. Bar = 100 μm or 20 μm in regular images or enlarged inserts. Dotted boxes indicate the typical morphologies on grooved PA gel.

labelled secondary antibodies in 1% BSA/PBS was then added and incubated at 37 °C for 1 h. After being washed five to seven times with PBS, the collected samples were incubated with Hoechst 33342 for 10–15 min at RT, washed three to five times with PBS, and then stored at 4 °C for examination by confocal laser scanning microscopy (Zeiss L710, Germany). The stained cells on PA hydrogel were examined immediately after staining.

H1 cells were stained with their typical biomarkers at the respective stages. Here, Alexa Fluor 488-conjugated rabbit polyclonal antibodies to OCT-4 (#5177) and Alexa Fluor 647-conjugated rabbit polyclonal antibodies to NANOG (#5448) (Cell Signalling Tech., Boston, MA, USA) were used for testing their stemness, while mouse mAbs to SOX17 (#Ab84990) and rabbit polyclonal antibodies to CXCR4 (#Ab2074) (Abcam, Cambridge, UK) were used for depicting definitive endodermal lineage. The corresponding DyLight 594-conjugated polyclonal Dnk-anti-rabbit (#Ab96921) and Alexa Fluor 488-conjugated polyclonal Dnk-anti-mouse (#Ab150109) antibodies (Abcam) were used as secondary antibodies. Rabbit polyclonal antibodies to albumin (ALB) (#Ab135575) with Alexa Fluor 488-conjugated polyclonal goat-anti-rabbit secondary antibodies (#Ab181448) and Alexa Fluor 647-conjugated rabbit mAbs to CK18 (#Ab194125) (Abcam) were used for verifying hepatocyte-specific functions. Image J Version 1.53c software (National Institutes of Health, Bethesda, MD, USA) was used to measure the mean fluorescence intensity for cell colonies at the STEM stage, and to quantify those values for individual cells at the DE and Pre-H stages, and for the cell layer at the M-H stage, all of which were normalized to the value of nuclei at each stage.

Simple western analysis

Cells at the distinct stages were harvested by trypsinization and washed with PBS. The collected cells were lysed in RIPA buffer supplemented with PMSF (Cell Signalling Technol.). The protein concentration of the lysates was quantified using a BCA assay kit (Pierce®, Thermo Scientific, USA). Capillary electrophoresis-based simple western (Wes) analysis was performed using the Wes device (ProteinSimple, San Jose, CA, USA) according to the manufacturer's protocol. In brief, the lysates were mixed with SDS-containing Sample Buffer to give a 1× final concentration and heated to 95 °C for 5 min. The total protein amount per 3 μl was listed for each antigen and the concentration of the related primary antibodies were optimized by pilot tests. HRP-conjugated mouse or rabbit secondary antibodies, chemiluminescence detection reagents and total protein labelling reagents were obtained from ProteinSimple. Data analysis was performed using the Compass software (Version 4.0.0, ProteinSimple). Each protein peak was analysed automatically and the median area under the peak was normalized first to GAPDH and then to the value on the planar substrate at different stages in some cases. The following primary antibodies used were from Cell Signalling Technol.: GAPDH rabbit polyclonal (#2118), OCT-4 rabbit polyclonal (#2750), NANOG rabbit polyclonal (#4903), SOX17 rabbit monoclonal (#81778), GATA6 rabbit polyclonal (#5851), ALB rabbit polyclonal (#4929), and CK18 mouse monoclonal (#4548) antibodies. Here one of the biomarkers at the DE stage was switched from CXCR4 to GATA6, simply because the anti-CXCR4 primary antibodies do not work well for the Wes tests.

RNA extraction and quantitative PCR test

Cultured cells on the last day of each stage were collected on various stiffnesses and topographies. Following the manufacturer's instructions, their total RNA was harvested using a RNA extraction kit (Tiangen, Beijing, China) with an in-column DNase digestion step. The corresponding cDNA was generated using a ReverTra Ace-α kit (Toyobo, Osaka, Japan) with 1 μg of RNA per reaction in a total volume of 20 μl. A reverse transcriptase-polymerase chain reaction was carried out using GoTaq® qPCR Master Mix by a two-step method according to the user manual (Promega, Madison, WI, USA) and then measured using a quantitative real-time amplification system (QuantStudio 7, Thermo Fisher). PCR reactions were performed at 95 °C for 2 min, followed by 40 cycles of 95 °C for 15 s, 60 °C for 60 s. A melting curve was run following each assay. The optimized primers for PCR tests are summarized in Table S1.†

Glycogen synthesis and indocyanine green (ICG) engulfment

Glycogen synthesis in HLCs was tested using a commercial kit and a periodic acid-Schiff stain (PAS) (Nanjing Jiancheng Bioengineering Institute, Nanjing, China). Briefly, the powders of periodic acid and Schiff's reagent were diluted in their respective diluting solutions to obtain their working solutions and then balanced at RT for 20 min. Cells were fixed with 95% ethanol for 2–5 min and washed for 1 min. The periodic acid solution was added to the fixed cells and incubated for 15 min. After being rinsed with water for 3–5 min, the Schiff's solution was added and incubated for 15 min, followed by washing for 30–60 s. Finally, the hematoxylin staining solution was added, incubated for 20–30 s, and flushed out. The stained cells were visualized using an optical microscope (Olympus IX71) at a magnification of 63×.

ICG engulfment by HLCs was also tested using a commercial kit (Sigma-Aldrich). Briefly, ICG powders were dissolved in water and diluted in a hepatocyte-differentiating medium at a final concentration of 1 mg ml^{-1}. The solution was added to pre-washed cells and incubated at 37 °C for 1 h. The washed cells were then fixed with 4% paraformaldehyde and rinsed before being visualized using an optical microscope (Olympus IX71) at 63× magnification.

Animal model and cell transplantation

Experiments were performed using female BALB/c nude mice aged five to seven weeks (Charles River, Beijing, China) and fed with a routine diet for one week before the CCl_4 treatment. CCl_4 (Solarbio, Beijing, China) was diluted using corn oil (Solarbio, Beijing, China) in 20% (v/v) and fully mixed using a magnetic stirrer for 4 h.[21] The CCl_4 solution was injected intraperitoneally at concentrations of 1.7–2.8 μl g^{-1} weight, with the mouse weight varying between 15 and 24 g. All mice were injected twice a week for four weeks. For liver injury repairing, about 10^6 HLCs differentiated from H1 cells on soft, planar PA

gel (referred to as Soft-P HLCs) or from routine polystyrene dishes (as control HLCs) were transplanted into the caudal vein using U-40 insulin pens (B|BRAUN, Melsungen, Hessen, Germany). Noting that Cell Tracker™ CM-DiI Dye is suitable for long-term labelling and tracking of cells,[22] injected HLCs were pre-stained with CM-DiI dyes (Invitrogen, Eugene, OR, USA) to conduct *in vivo* tracking by confocal laser scanning microscopy (Zeiss L880, Germany), where the mouse was anesthetized using phenobarbitone on Day 4 or 14 after cell transplantation to open the abdomen and expose the liver for examination. The structures of the liver and its edges were recognized by the liver autofluorescence, while H1 cell-derived HLCs residing in the liver were identified using CM-DiI.

The progress of mouse liver injury and repair was monitored periodically. At given time points during CCl_4 injection, the whole blood was suctioned by capillary from the inner canthus vein. The serum was collected by centrifugation at 3500 rpm (1150*g*) for 10 min at 4 °C after 4 h standing at RT, and then stored at −80 °C for subsequent analyses. The activities of alanine aminotransferase (ALT) and aspartate aminotransferase (AST) were tested using the corresponding kits (Sigma-Aldrich). Four weeks after CCl_4 injection, the liver was removed and paraffin-embedded for hematoxylin and eosin (H&E) or Masson staining. All the tests were conducted at the endpoint of an additional four weeks of post-HLC transplantation to ascertain the repairing of liver injury.

Statistical analysis

For comparisons between any two groups, a Student's *t*-test was performed if the data passed the normality test, or the Mann–Whitney test was used if not. A one-way test followed by the Holm–Sidak test was performed to determine the statistical significance of multiple-group comparison. If the normality test (Shapiro–Wilk) failed, a one-way ANOVA on Ranks followed by Dunn's test was used. A two-way ANOVA test followed by the Holm–Sidak test was used to test the statistical significance of differences in the measured parameters between the two factors, substrate stiffness and topography. *P* values less than 0.05 were considered statistically significant.

Results

hESCs are able to grow and undergo hepatic differentiation on various PA substrates with inducing factors

The *in vitro* differentiation of ESCs into different lineages relies on effective stimulation of the *in vivo* milieu, including both biochemical factors and mechanical or physical cues. While hepatic differentiation of hESCs generally undergoes sequential stages on the extremely stiff substrate of culture dishes,[2] here we modified this four-stage, feeder cell-free strategy to induce hepatic differentiation of H1 cells on relatively softened PA hydrogels with the respective inducing factors accordingly in four topographies (Fig. 1a).[2,6,23] Here the application of these topographical configurations is mainly based on our previous works on understanding how substrate topography regulates the stemness maintenance and directed differentiation of stem cells, where similar topographies are applied.[13,19] We first used actin staining (white arrows) to illustrate profound morphological changes on varied PA gels at four distinct stages, where nucleus staining served as references (red arrows) (Fig. 1b). H1 clones effectively adhered to the substrate and sustained normal growth, which is a prerequisite for maintaining their stemness. Typically, on a grooved hydrogel (dotted boxes in Fig. 1b and Fig. S1a†), H1 clones or differentiated cells grew with their characterized morphologies at the respective stages, that is, forming isolated, compact colonies with a small fraction of cells having a high nucleus-to-cytoplasm ratio and prominent nuclei at the STEM stage, starting to spread out into a loose clonal structure with less visible boundaries and increased individual spindle cells at the periphery at the DE stage, becoming a flattened and widely-spread layer with tight intercellular connections at the Pre-H stage, and fully spreading across multiple topographical elements into a complete monolayer with tightly connected cells displaying cuboidal or polygonal appearances and sharing enlarged or bi-nucleated nuclei at the M-H stage. Similar features were observed when the cells were placed on other topographical substrates (Fig. 1b). All individual cells inside H1 clones or aggregates presented clear boundaries and visible nuclei (enlarged inserts at the upper left corner of each panel). These observations indicated that H1 cells are able to grow on topographical PA hydrogels and to implement hepatic differentiation with the respective inducing factors and that our protocol seemed to represent well the *in vivo* mechanical or physical microenvironment in liver sinusoids.

Similar morphologies of H1 clones or cells at the four stages were also observed from the optical images (Fig. S1a†). Morphological analysis of H1 clones at the STEM stage (solid box) was further performed to quantify their dependence on the substrate stiffness or topography. The clones presented a high aspect ratio value in the grooved configuration but a low value in the hexagonal one (Fig. S1b†), which is opposite to the topography dependence of the clone circularity according to the parameter definitions (Fig. S1c†). Compared with those on stiff substrates, the clones on soft substrates yielded a slightly lower aspect ratio in the grooved configuration but a higher aspect ratio in the hexagonal configuration. No significant difference was found in the clone area and number at the same seeding density (Fig. S1d and e†), supporting the consistency of the clone formation capacity on varied PA hydrogels. These results indicated that the substrate guidance usually used for individual cells also applies for the growth and differentiation of H1 clones. Substrate topography is a key factor in controlling the morphology of H1 clones, in which the grooved configuration exhibits the greatest effect to align the clones or cells. In addition, SEM imaging illustrated that massive ECM proteins were produced at the latter two stages, tending to wrap the cells into a thin layer and displaying the lamellipodia at the curling periphery of the clone (arrows in Fig. S2†), as observed.[24]

Substrate stiffness dominates fate decision of hESCs in hepatic differentiation

Substrate stiffness governs the fate decision of stem cell differentiation.[25,26] Here we first tested the roles of substrate stiffness in hepatic differentiation of H1 cells on planar PA gels at distinct stages. At the STEM stage, the two stemness transcription factors OCT-4 and NANOG were well expressed spanning over the entire clone on both stiff and soft substrates and uniformly distributed inside the clone, even with random differences in immunostaining from one region to another (Fig. 2a). Their expressions seemed higher on the stiff substrate, implying that high stiffness may favor the maintenance of stemness. At the DE stage, the two DE biomarkers *SOX17* and *CXCR4* were well stained over the entire clone with a high intensity at the periphery and highly co-localized in the cell body (Fig. 2b). Again, high expressions on the stiff substrate proposed the capacity of stiffness-enhanced DE differentiation. At the M-H stage, the two hepatic biomarkers *ALB* and *CK18* were uniformly distributed inside the cells and were present over the entire cells in a sheet-like manner when the cells became larger and tightly connected (Fig. 2c). Moreover, the soft substrate seemed favorable for the final-stage hepatic differentiation.

The above biomarker expressions were further quantified by immunostaining, immunoblotting and qPCR tests. At the protein level (Fig. 2), the relative fluorescence intensity (RFI) per clone/cell was normalized to the value on the planar, stiff substrate for each biomarker. Data indicated that OCT-4 and NANOG expressions were relatively higher on the stiff substrate than those on the soft substrate at the STEM stage (Fig. 2d). Similar results were obtained for *SOX17* and *CXCR4* at the DE stage (Fig. 2e). Such differences between the two stiffnesses were reversed at the M-H stage where *ALB* and *CK18* expressions were relatively higher on the soft substrate than those on the stiff substrate (Fig. 2f). Immunoblotting tests confirmed the above observations for these biomarkers at the three stages (Fig. 2g–l). At the gene level (Fig. 3), relatively high expressions of *OCT-4* and *NANOG* at the STEM stage (Fig. 3a) and *SOX17* and *CXCR4* at the DE stage (Fig. 3b) and low expressions of *ALB* and *CK18* at the M-H stage (Fig. 3c) were observed on the stiff substrate compared to those on the soft substrate, which were similar to the protein expression patterns but with less significant differences. An exceptional case was the slightly higher *CXCR4* expression on the soft substrate without a significant difference between the stiff and soft substrates. Thus, these data suggested that H1 cells are favored to maintain their stemness and mediate DE differentiation on stiff substrates, and differentiate into HLCs on soft substrates.

Substrate topography assists hepatic differentiation of hESCs on PA gels

Substrate topography is also crucial in supplementing the directed differentiation of stem cells.[19,27] At the STEM stage, OCT-4 and NANOG were expressed in the nuclei or specifically in the cytoplasm (*i.e.*, NANOG) and co-localized over the entire clone especially on the grooved or pillar substrate. Specifically,

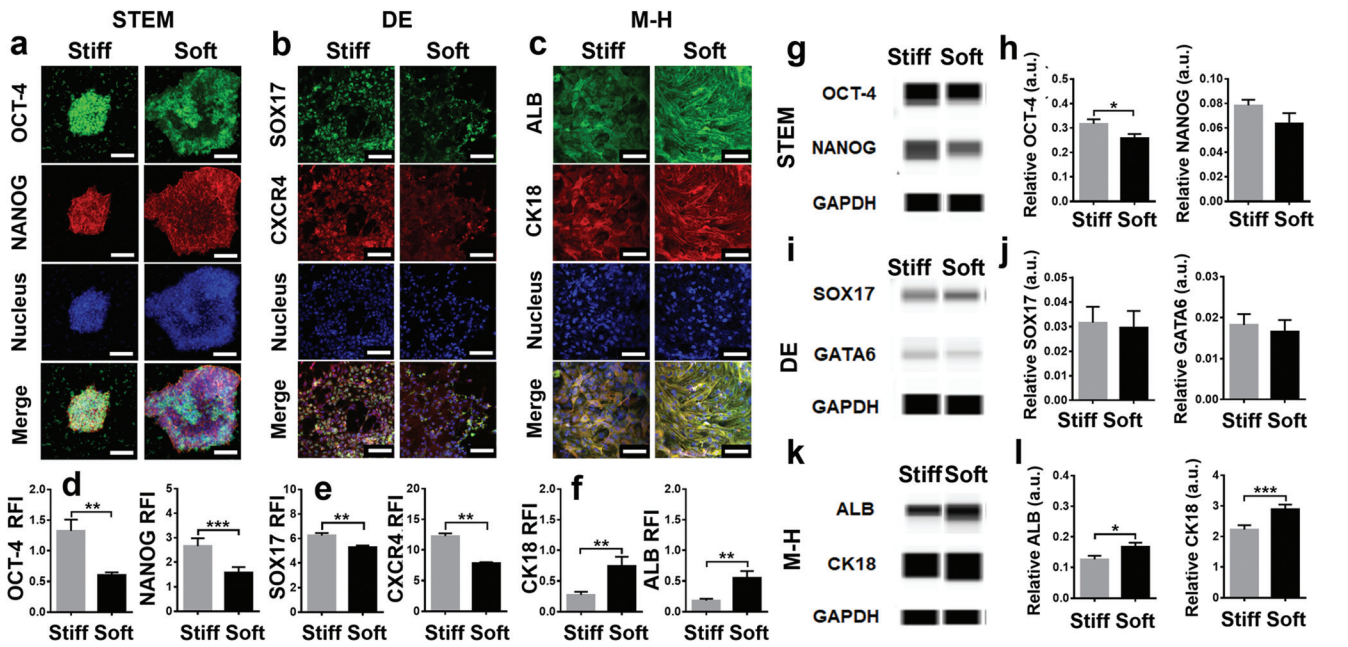

Fig. 2 Impacts of substrate stiffness on stage-specific biomarker expressions at the STEM, DE or M-H stage with same planar topography. (a–f) Typical images of OCT-4 and NANOG (a), SOX17 and CXCR4 (b), or ALB and CK18 immunostaining (c) at the respective stages and their relative fluorescence intensities quantified from >30 fields-of-view (FOVs) in triplicate repeats (totally >200 cells) (d–f). Data were presented as mean ± SE (per clone at the STEM or per cell at the DE or M-H stage). Bar = 100 μm. (g–l) Typical Wes images of OCT-4 and NANOG (g), SOX17 and GATA6 (h), or ALB and CK18 immunoblotting (i) at the respective stages and their relative optical intensities (a.u.) quantified in 5–10 repeats (j–l). Data were presented as mean ± SE. *, **, or ***, $P < 0.05$, 0.01, or 0.001 (*t*-test).

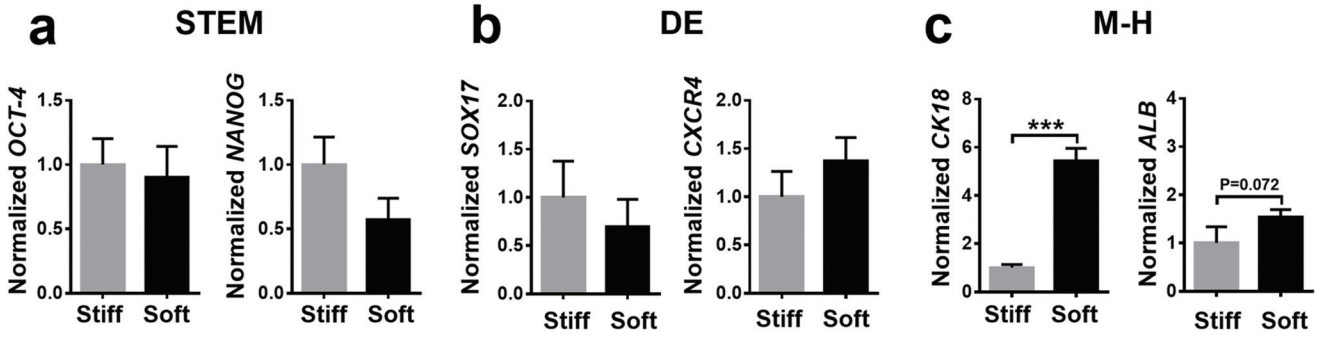

Fig. 3 Impacts of substrate stiffness on stage-specific gene expressions at the STEM, DE or M-H stage in same planar topography. Typical genes *OCT-4* and *NANOG* (a), *SOX17* and *CXCR4* (b), or *ALB* and *CK18* (c) were analyzed by qPCR tests and their relative transcription levels were quantified in 3–8 repeats. Data were normalized by the one on stiff gel (Stiff-P) after being calculated by their respective reference genes and presented as the mean ± SE. ***, $P < 0.001$ (*t*-test).

these two biomarkers tended to be uniformly distributed on the grooved (2nd column) or hexagonal (4th column) substrate where the nuclei likely settled down into the pits. In contrast, they seemed to form clusters on the square pillar one (3rd column) when the cells were likely to stick to the ridges, suggesting that the expression of pluripotent biomarkers is sensitive to the topography guidance, especially for those on soft gel (Fig. S3a and S4b†). At the DE stage, SOX17 and CXCR4 expressions were more sensitive to the topography guidance with augmented alignment, as exemplified in high intensity in the cell body as well as their nuclei embedded in the low pit of the grooved (2nd column), square pillar (3rd column), or especially hexagonal (4th column) configuration on soft gel (Fig. S3b and S4b†). At the M-H stage, ALB and CK18 expressions were less sensitive to the topography guidance and tended to be uniformly distributed over the entire cell in a sheet-like manner, especially on the planar substrate (Fig. S3c and S4c†). These observations implied that the substrate topography is correlated with the potential of hepatic differentiation of H1 cells.

To quantify the effects of topographical PA gels, the H1 clone circularity at the STEM stage was used as a measure to compare their stemness maintenance and differentiating potential on varied topographies. This is because, no matter how many variables, including the shape and size of the ridge, the spacing size between the neighboring ridges, and the depth of the pit, are assumed to govern the substrate topographical circularity, the actual biological responses are determined by stable morphologies of the seeded clones or cells on topographical substrates, serving as the starting point for the following hepatic differentiation. As such, the clone circularity read a monotonic increase from the grooved through pillar to the hexagonal configuration while the planar one served as the control (Fig. S1c†). Again, the stage-specific biomarker expressions were tested using immunostaining, immunoblotting and qPCR tests (Fig. 4, 5 and Fig. S3, S4†) at the protein and gene levels and all measured data were normalized to the one on the planar substrate at the same stiffness. At high stiffness (stiff PA gel at 46.7 kPa), OCT-4 and NANOG expressions at the STEM stage were indifferent at the protein level with varied circularities (Fig. 4a and b). Relatively high *OCT-4* or *NANOG* expressions were observed in the hexagonal or square pillar configuration, seemingly increasing with the circularity (Fig. 4c). Interestingly, SOX17 and CXCR4 (or GATA6) expressions at the DE stage were monotonically increased with increase of circularity (Fig. 4d and e), similar to the pattern of the relevant gene expressions (except for the highest *CXCR4* expression in the square pillar configuration) (Fig. 4f). In contrast, ALB and CK18 expressions at the M-H stage were monotonically decreased with increase of circularity (Fig. 4g and h), which is consistent with the pattern of the relevant gene expressions (Fig. 4i). These results implied that the substrate topography plays complementary roles on PA gel at different stages in directing hepatic differentiation.

At low stiffness (soft PA gel at 6.1 kPa), the impacts of substrate topography were relatively complicated at the STEM stage. OCT-4 and NANOG expressions at the protein level were first increased with circularity but declined to the similar levels to the ones for planar control, while their gene expressions fluctuated within a factor of two (Fig. 5a–c). Importantly, SOX17 and CXCR4 (or GATA6) expressions at the DE stage were monotonically increased (Fig. 5d–f) but ALB and CK18 expressions at the M-H stage were monotonically decreased (Fig. 5g–i) with increase of circularity at both protein and gene levels. In addition, the dependence of ALB or CK18 expression on circularity at the Pre-H stage seemed to be in between the DE and M-H stages without monotonic alterations (Fig. S5a–c†). Collectively, increasing the H1 clone circularity favors stemness maintenance potential and DE-lineage differentiation but compromises hepatic differentiation on either stiff or soft PA gel substrates.

To optimize the hepatic differentiation of H1 cells on PA gels, the coupling effects of substrate stiffness and topography were also tested by comparing the differences of the grouped data at the respective stages. Here we pooled all the data together from varied stiffnesses and topographies, *i.e.*, eight cases at each stage, by assuming that all of them yielded the

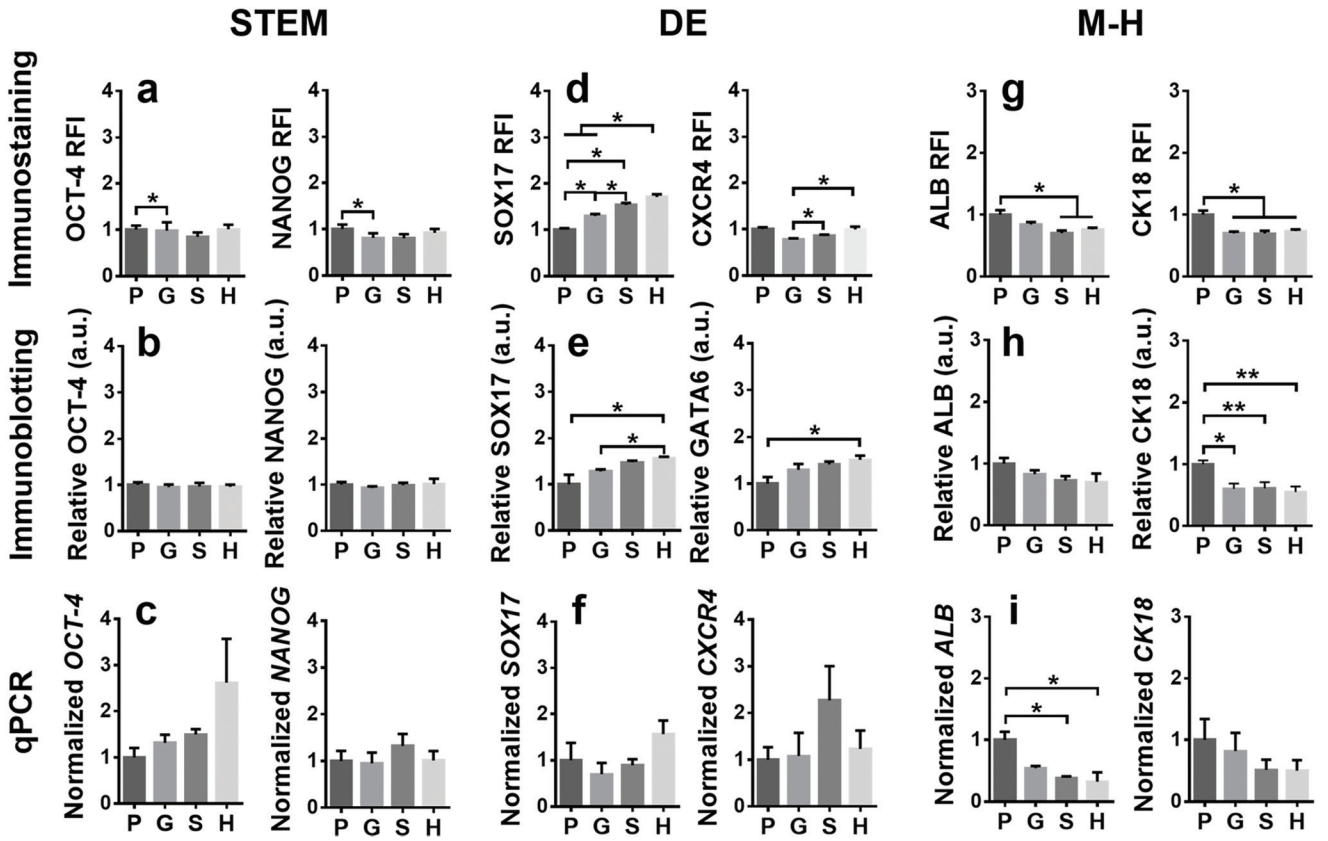

Fig. 4 Impacts of substrate topography on stage-specific protein or gene expressions at the STEM, DE or M-H stage on stiff PA gel. Typical biomarkers of OCT-4 and NANOG (a–c), SOX17 and CXCR4 (or GATA6) (d–f), or ALB and CK18 (g–i) at the respective stages were analyzed. Data were obtained from immunostaining (1st row), immunoblotting (2nd row), or qPCR (3rd row) tests in at least triplet repeats and presented as mean ± SE after being normalized by the one on planar gel. * or **, $P < 0.05$ or 0.01 (one-way ANOVA).

same weights in regulating hepatic differentiation. A two way ANONA test was further conducted between any paired values of three data sets of immunostaining, immunoblotting, and qPCR tests, *i.e.*, two biomarker and two gene expressions per case, with all data being normalized to the one on stiff, planar PA gel at that stage. The analysis indicated that the contributions of substrate stiffness and topography were coupled to a certain extent, as seen in significantly different cases of stage-specific biomarker and gene expressions (Table S2†). Typically, high OCT-4 expression in the square pillar configuration was visualized, not only on soft but also on stiff gel, at the STEM stage. SOX17 expression was increased with increase of clone circularity on stiff gel, all of which were higher than those on soft gel with a similar monotonic increase pattern at the DE stage. ALB expression was decreased with increase of clone circularity on stiff gel, all of which were lower than those on soft gel with a similar monotonic decrease pattern at the M-H stage (not all the statistical data of paired comparisons are shown in Table S2† for clarity; refer to similar data sets in Fig. 4 and 5 for details and Fig. S8 and S9† for all semi-quantitative immunostaining and immunoblotting). Thus, these coupling effects could help optimize the hepatic differentiation of H1 cells.

hESC-derived HLCs on PA gels are functional *in vitro* and *in vivo*

We next conducted functional tests for HLCs derived from H1 cells on various PA gels. Here three data sets were integrated to evaluate their functionality at the M-H stage. First, typical drug metabolism indicated that the concentrations of CYP450 1A2 and 2D6 metabolites were higher on the soft substrate than those on the stiff substrate (Fig. 6a and b), supporting the above observations of low stiffness-favored hepatic differentiation (Fig. 2 and 3). Applying a planar PA gel seemingly favored the functionality with the highest CYP450 metabolism, also imparting the aforementioned clone circularity-dependent hepatic differentiation on the soft substrate (Fig. 4 and 5). Second, the typical cellular staining for glycogen synthesis was visible on all substrates at the M-H stage (Fig. 6c), indicating that the HLCs are potentially functional in glycogen synthesis. Synthesized glycogens were likely present at the vicinity of the nuclei on soft PA gels (arrows and arrowheads). Third, the typical ICG engulfment was evident at the M-H stage (Fig. 6d), presenting the disperse distribution on stiff gel but the concentrated distribution on soft gel (arrows and arrowheads). This phagocytic capacity seemed higher in the planar configur-

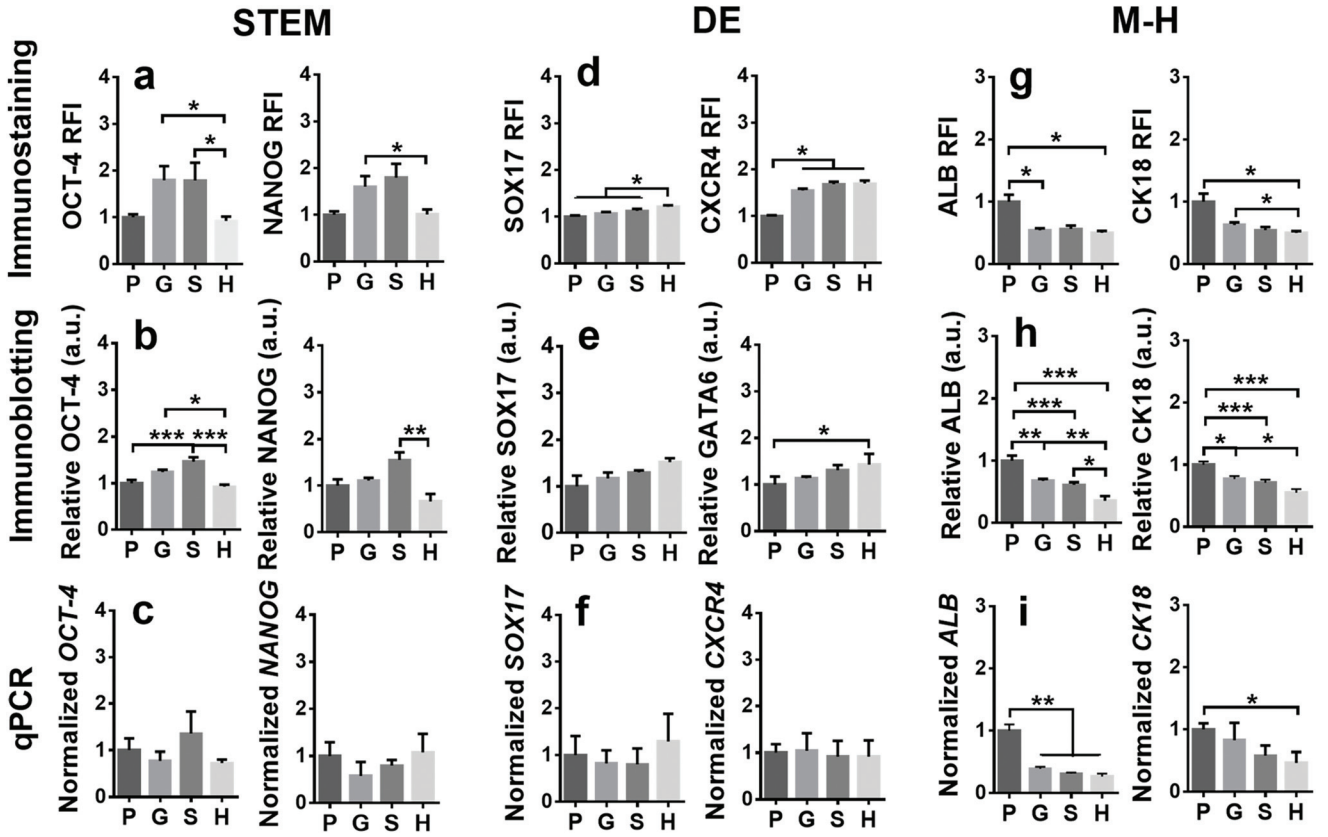

Fig. 5 Impacts of substrate topography on stage-specific protein or gene expressions at the STEM, DE or M-H stage on soft PA gel. Typical biomarkers OCT-4 and NANOG (a–c), SOX17 and CXCR4 (or GATA6) (d–f), or ALB and CK18 (g–i) at the respective stages were analyzed. Data were obtained from immunostaining (1st row) or immunoblotting (2nd row), or qPCR (3rd row) tests in at least triplet repeats and presented as mean ± SE after being normalized by the one on planar gel. *, **, or ***, $P < 0.05$, 0.01, or 0.001 (one-way ANOVA).

ation on soft gel. Similar results of glycogen synthesis and ICG engulfment were also obtained at the Pre-H stage with significantly reduced staining on stiff gel (Fig. S5f–g†). Collectively, HLCs on the soft, planar substrate presented higher drug metabolism and stronger glycogen synthesis and ICG engulfment compared to those in the other three topographies or all on stiff gel, supporting the coupling effects of substrate stiffness and topography on hepatic-specific functions. Thus, the HLCs derived from PA gels are likely functional with a monolayer-like morphology and relatively softened feature, consistent with the fact that cells prefer to survive and maintain their biological characteristics in the environment which is similar to their environment.[28]

To further test the functionality of differentiated HLCs regulated by substrate stiffness and topography, a mouse transplantation model of CCl_4-induced liver injury was used, since the transplanted cells have an advantage of repairing liver injury.[29] Here two types of HLCs, one optimized from soft, planar PA gels (as Soft-P HLCs) and the other derived from conventional differentiation (as control HLCs), were transplanted into CCl_4-treated mice (Fig. 7a) while feeding wild type (WT) mice *via* the same protocol without transplanting HLCs. Here control HLCs were obtained from the same four-stage protocol on a matrigel-coated polystyrene dish[2,6,23] and then confirmed using similar tests as Soft-P HLCs on PA gels (Fig. S6†), prior to cell transplantation. In CCl_4-treated mice, the histological and histochemical staining revealed the serrated edges, ballooning degeneration (arrows), apoptotic cells (arrowheads) and remarkably increased collagen fibers (swallowtail) (Fig. 7b), and the serum tests showed enhanced AST and ALT activities (Fig. 7c and d), confirming that the liver injury mouse model was successfully developed. After Day 4 or 14 of cell transplantation, more Soft-P HLCs were able to quickly enter into the host liver (Fig. 7e) with obvious proliferation (Fig. 7f) compared to the control HLCs in WT or CCl_4-treated mice. Hepatocyte autofluorescence illustrated that, compared with numerous necrotic hepatocytes in CCl_4-treated mice, the number of necrotic hepatocytes was reduced remarkably when transplanting control HLCs or even further decreased when transplanting Soft-P HLCs. In contrast, the surface roughness and the jagged edge of the injured liver were altered significantly in HLC-transplanted mice compared to CCl_4-treated mice (Fig. 7g). Randomly-selected optical images of the tested livers are shown in Fig. S7† for reference, especially illustrating the smoother surface of the liver tissue with Soft-P HLC injection (last column in Fig. S7b†). This turnover was confirmed

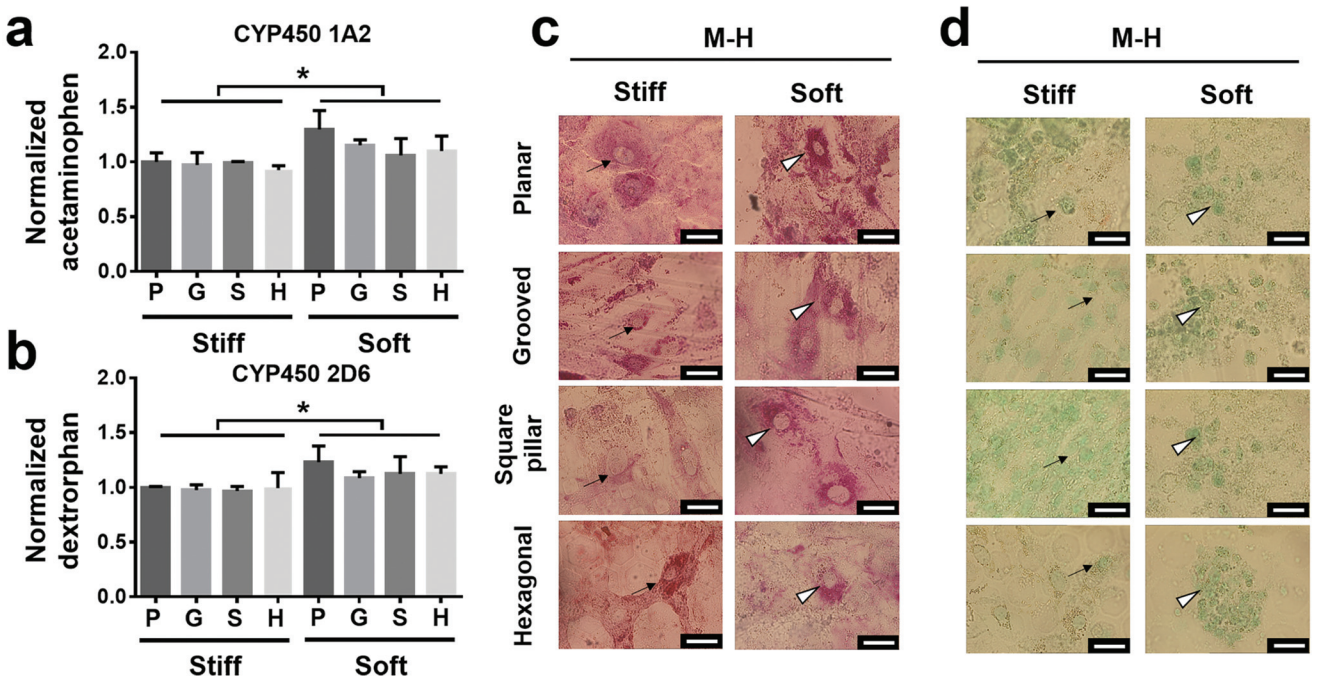

Fig. 6 Functional tests of H1 cell-derived HLCs on PA gels on Day 16 at the M-H stage. (a and b) Liver-specific metabolic products of phenacetin (Acetaminophen, for CYP1A2 activity) (a) and dextromethorphan (dextrorphan, for CYP2D6 activity) (b) were determined by liquid chromatography-tandem mass spectrometry of collected supernatants. Plotted were the mean ± SE of normalized drug metabolism and statistical analysis was performed by two-way ANOVA. n = 2–4. (c and d) Typical histochemical staining images of glycogen synthesis (c) and ICG phagocytosis (d). Arrows or arrowheads indicate the differences on a stiff or soft substrate, respectively. Bar = 100 μm. *, $P < 0.05$ (two-way ANOVA).

by histological or histochemical staining and serum tests at Day 30 post-transplantation (Fig. 7h–j). Here, the fibrotic phenotype of the injured livers in CCl_4-treated mice was partly reversed by injecting control HLCs and significantly recovered by injecting Soft-P HLCs (Fig. 7h). Furthermore, the AST activity after injecting Soft-P or control HLCs into CCl_4-treated mice was significantly reduced to even close to normal levels similar to those in WT mice (Fig. 7i). Again, the ALT activity was lowered remarkably with Soft-P HLC transplantation to the level similar to that in WT mice (Fig. 7j). Collectively, these tests using CCl_4-treated mice indicate that the liver injury was remarkably repaired with Soft-P HLC transplantation, implying the potential application of regulating the stiffness and topography of PA gels.

Discussion

Directed differentiation of stem cells provides the basis for the development, growth, and repairing of living organisms. This work aims at elucidating the mechanical or physical regulation of hepatic differentiation of hESCs on substrates with systematically-varied stiffnesses and topographies that represent the typical physiological niches in the liver.

Our data indicated that the substrate stiffness is dominant in this process, in which the stiff substrate favors stemness maintenance and DE differentiation while the soft substrate is preferred in hepatic differentiation. Substrate topography assists the stemness maintenance and directed differentiation, where high clone circularity (*e.g.*, on the square pillar or hexagonal substrate) promotes stemness maintenance or DE lineage but low clone circularity (*e.g.*, on the grooved substrate) augments hepatic differentiation. Moreover, the differentiated HLCs exhibit the typical functions of hepatocytes, as can be seen that the substrate stiffness and topography cooperatively regulate liver-specific drug metabolism, glycogen synthesis and ICG engulfment and the transplantation of substrate-optimized HLCs favors the repairing of CCl_4-induced liver injury in mice. While a body of evidence indicates that the substrate stiffness and topography direct the differentiation of somatic stem cells,[19,30] our results provide the first evidence that the coupling of substrate stiffness with substrate topography serves as the key regulator in the hepatic differentiation of hESCs. A working model was then proposed to illustrate how these mechanical or physical factors cooperatively manipulate the *in situ* continuous hepatic differentiation of H1 cells (Fig. 8).

hESCs undergo proliferative growth and stemness maintenance in their anchoring niche that could be depicted as varied stiffnesses and topographies. Substrate stiffness is a primary factor in stemness maintenance and directed differentiation of hESCs. Here, both soft and stiff PA planar hydrogels are favorable for OCT-4 and NANOG expressions at the gene or protein level (Fig. 2 and 3), supporting that soft substrates in several or several-tens of kPa enable mESCs to form undifferentiated clones, retain high-levels of OCT-4 and NANOG expression,

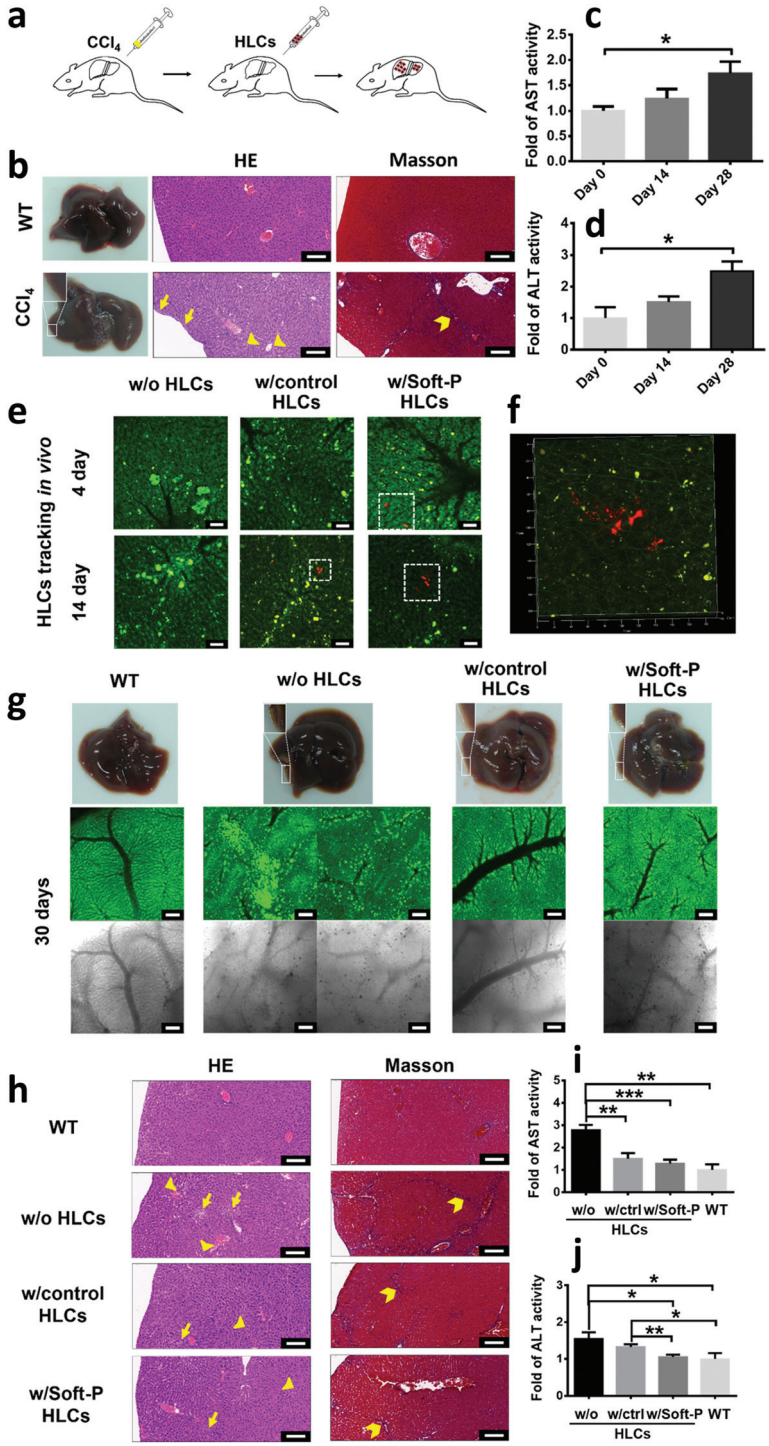

Fig. 7 Transplantation of optimized HLCs in CCl_4-treated mice. (a) Schematic of preparing the mice with liver injury and HLC transplantation. (b) Typical liver images with or without CCl_4 treatment. White box with the enlarged image in the left lower panel denote the serrated edges and rough surfaces of injured livers. Arrows indicate the ballooning degeneration and arrowheads point the apoptotic cells in HE staining in the middle lower panel. Swallowtail in the right lower panel depicts the collagen fibers in Masson staining. Bar = 100 μm. (c and d) AST (c) and ALT (d) activities in CCl_4-treated mice measured by ELISA assay and normalized to the values from wild type (WT) mice at the midpoint and endpoint of four-week injection. n = 3. (e and f) *In vivo* tracking of CM-DiI -stained HLCs (red) and autofluorescent primary hepatocytes (green) using confocal microscopy on Day 4 or 14 in WT mice, CCl_4-treated mice, and CCl_4-treated mice transplanted with control or Soft-P HLCs (e). Enlarged boxes indicate the resided and rescued HLCs (f). Bar = 50 μm. n = 2. (g) Typical liver images after HLC injection in CCl_4-treat mice. 1st row indicates typical liver images of WT mice, and 2nd row denotes the serrated edges and rough surfaces of injured livers, 3rd or 4th row denotes the CCl_4-treated mice transplanted with control or Soft-P HLCs on Day 30 of autofluorescent primary hepatocytes (green) or DIC images, respectively. Bar = 100 μm. n = 3–6. (h) HE and Masson staining on Day 30 after injection. Bar = 100 μm. n = 3–6. (i and j) AST (i) and ALT (j) activities in CCl_4-treated and HLC-transplanted mice measured by ELISA assay and normalized to the values of WT mice on Day 30 after injection. *, **, or ***, P < 0.05, 0.01, or 0.001 (t-test).

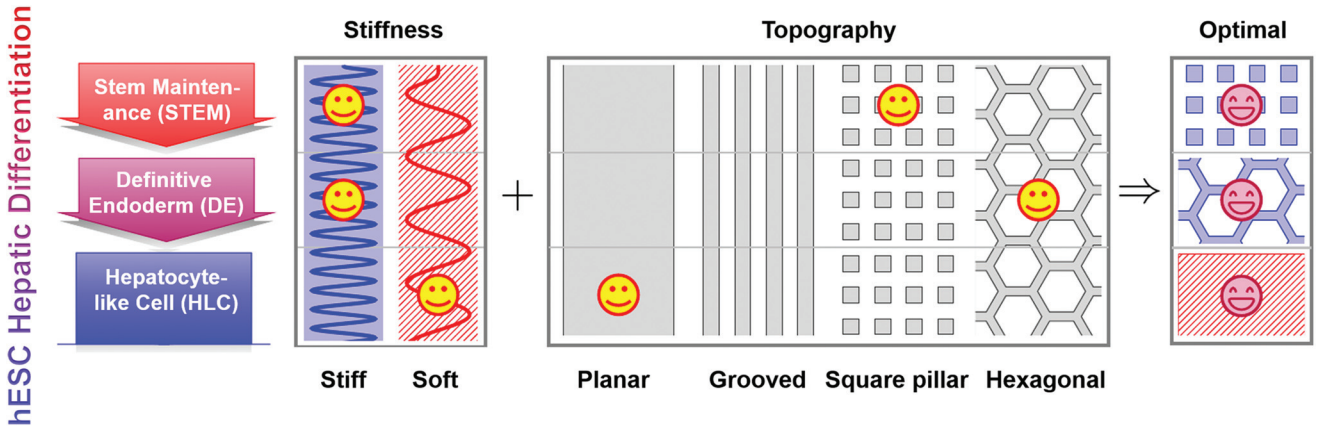

Fig. 8 A working model proposed for illustrating the coupled impacts of substrate stiffness and topography on hepatic differentiation of H1 cells. Here are two key points: (1) Substrate stiffness dominates hepatic differentiation of hESCs, in which stiff substrates favor stemness maintenance and DE differentiation while soft substrates promote Pre-H and M-H differentiation. (2) Substrate topography assists hepatic differentiation of hESCs, where the square pillar, hexagonal, and planar configurations are favorable, respectively, to stemness maintenance, definitive endoderm specification, and hepatocyte-like cell maturation.

and induce embryoid bodies or organoid tumors.[31] In fact, hESCs are sensitive to mechanical or physical microenvironments when the cells are placed on micropatterned surfaces, where high stiffness enhances cellular traction force *via* cytoskeletal remodelling and fosters cell–cell mechanotransduction through E-cadherin.[32] Our data present the clear contour, sufficient height, and tight cell–cell connection, as well as the efficient ECM deposition in H1 clones at a given stiffness (Fig. 1 and Fig. S1, 2†), which is also in accordance with the above measurements. Meanwhile, different substrate stiffnesses also direct early differentiation of hESCs in distinct ways. Stiff, intermediate, and soft substrates are known to work for mesodermal, endodermal, and ectodermal differentiation,[13,33] consistent with our findings in DE differentiation at an intermediate stiffness of 6.1 or 46.7 kPa. The stiffness dependence still exists even at these intermediate stiffnesses, as indicated by the favored DE differentiation of H1 cells on relatively stiffer substrates (Fig. 2 and 3). This less than ten-fold variance of substrate stiffness is biologically meaningful, as seen in the similar stiffness changes of liver tissues when progressing into a fibrotic or cirrhotic liver.[34] Moreover, the elasticity of normal tissues does not vary sharply over three or four orders-of-magnitude, implying that using a conventional polystyrene dish for the directed differentiation of hESCs *in vitro* might be too stiff to maintain the phenotypes of target cells.

Differential contributions of topographical substrates are also found to manipulate stem cell stemness and directed differentiation. For mESCs, a relatively flattened colony is formed on a groove or square pillar configuration and a spheroid colony on a hexagonal configuration, and their stemness is likely maintained in the hexagonal or square pillar configuration.[13] For hESCs, a square pillar configuration is found to be advantageous to maintain their stemness (Fig. 4 and 5) on a soft or stiff substrate, supporting that hESCs could adapt well to a square pillar configuration and maintain their stemness for weeks.[35] Morphologically, the groove configuration guides the formation of long, narrow colonies with stable stemness (Fig. 1 and Fig. S1, 2†), consistent with the previous observations.[36] Definitive endodermal differentiation of hESCs is indispensable for harvesting mature hepatocytes, in which substrate topography also plays a critical role. For example, hESCs tend to differentiate into endodermal cells on thin fibrils (<400 nm) but into ectodermal cells on thick ones (>400 nm).[12] Similarly, small-sized embryoid bodies placed on micropatterned islands promote endodermal differentiation with high expressions of SOX17 and CXCR4.[37,38] While it is difficult to quantify the effects of substrate topography, here we defined a parameter of the circularity of H1 clones initially formed. It is interesting that, no matter what the actual shape and geometry of PA gels are, DE differentiation of H1 cells is promoted with high clone circularity (Fig. 4, 5 and Fig. S1, 2†). In fact, the reasons for choosing these four substrate configurations mainly lie in two aspects: one is based on the physical cues in the liver where various topographies exist. For example, the grooved one tends to represent the plate-like structures of the residing hepatocytes, the square pillar one may imitate the mechanical support of the disperse hepatic stellate cells in the Disse space, and the hexagonal one attempts to illustrate the typical shapes of non-mesenchymal cells in the sinusoids. The other is derived from our previous works on elucidating how substrate topography regulates the stemness and differentiation of ESCs, where similar typical topographies have been applied.[13,19] This measure seems simple and practical and could be more physiologically relevant. Nevertheless, the four topographies used in this work are largely simplified from *in vivo* anatomical structures, even though their key features were characterized in the current configurations. Effects of physiologically-mimicking combinations of these topographical elements need to be elaborated in future works.

Furthermore, substrate stiffness is combined with substrate topography to direct hepatic differentiation of hESCs. While previous studies mainly focus on various cultures such as embryoid body formation, single cell culture, suspension or 3D culture, and additive factors,[39] little is known about how mechanical or physical cues manipulate this process. Our data indicated that a planar configuration is advantageous to hepatic differentiation of hESCs at either the Pre-H or M-H stage (Fig. 2–5). This topographical contribution is coupled with the impact of substrate stiffness, as exemplified by how a square pillar configuration is favorable on soft but not stiff substrates. In fact, soft substrates are more favorable in targeting the differentiation of HLCs in the same configuration, matching well with the soft liver tissue *in vivo*. On the other hand, the hepatic phenotype of these differentiated cells is critical since existing evidence indicates that HLCs derived from differentiated hESCs are only partially mature and show limited functions of primary hepatocytes.[40] In the current work, the two typical biomarkers ALB and CK18 were selected to confirm the hepatic phenotype of these differentiated cells (Fig. 2–5) even though more hepatic biomarkers are helpful to identify their phenotype at the protein or gene levels.[41,42] The collected HLCs exhibited higher CYP450 metabolism, glycogen synthesis and ICG engulfment levels at the M-H stage (Fig. 6), implying that these cells show liver-specific functions, at least partially. In fact, the HLCs harvested from a soft, planar PA gel significantly attenuated liver injury and alleviated its fibrosis-like symptoms (Fig. 7), thereby confirming the availability of PA gel-optimized HLCs from H1 cells *in vivo*. These results are also consistent with existing evidence that the HLCs are favored to repair liver injury, regardless of various inducing factors.[43–45] We also found that these HLCs are able to survive up to thirty days with a well-defined hepatocyte-like morphology, smooth edges of liver tissue, thin collagen fibrils, and low AST activity, as compared with WT healthy mice, which promotes the turnover of CCL_4-induced liver injury. While 100% maturity of hepatocytes are extremely challenging for *in vitro* procedures, the collected HLCs in the current work are, at least, partially mature in repairing CCl_4-induced liver injury, with combined substrate stiffnesses and topographies.

Elucidating these coupling effects of substrate topography and stiffness is biologically relevant when they are designed to mimic the hepatic microenvironment *in vivo* or to reconstruct the engineered liver organoid *in vitro*. On one hand, the implementation of hepatocyte functions is also sensitive to substrate stiffness, especially when the stiffness matches liver tissue *in vivo*. Soft supports with a stiffness of several kPa provide an appropriate environment for albumin synthesis, which is five-fold higher than cells with a stiff support with a stiffness of several-tens of kPa.[46] Noting that the soft substrate likely corresponds to the elasticity of normal liver tissue and the stiff one corresponds to that of a cirrhotic liver or liver tumors,[47,48] these easily tunable PA hydrogels could provide a workable platform *in vitro* for reconstructing liver tissues or organoids or screening the candidate drugs for liver diseases. Our data also indicated that hESCs are readily directed into precursor hepatocytes or HLCs on PA hydrogel and that soft substrates are favorable for ALB and CK18 expressions, CYP450 metabolism, glycogen synthesis, and ICG engulfment (Fig. 6 and Fig. S5†). On the other hand, substrate topography defines the cell morphology and alters liver-specific functions. A sub- or super-cellular pore size on porous collagen foams promotes hepatocellular differentiation by confining 2D cell spreading or affecting 3D intercellular contacts, while intermediate pore sizes inhibit hepatic differentiation by promoting 2D cell spreading.[49] These simple porous scaffolds can be evolved to more complicated 3D matrices with a similar architecture to *in vivo* liver tissue, which enables hepatocytes to be cultured in different topographies and porous matrices.[50] Our data indicated that H1 clones or cells prefer to grow on the ridge of grooves, align into the pit between pillars, or present either on the top or in the pit of hexagons (Fig. 8 and Fig. S1–3†). Moreover, these substrate-optimized HLCs on topographical PA hydrogel also support liver-specific functions (Fig. 6 and 7).

Conclusions

Collectively, the mechanical or physical cues of PA hydrogel substrates on which hESCs are placed differentially manipulate their hepatic differentiation. H1 clones or cells are favored to maintain their stemness and undergo DE differentiation on stiff substrates but differentiate into HLCs on soft substrates. They also prefer to maintain their stemness on high clone circularity but promote hepatic differentiation on low clone circularity. Considering the cooperative effects of the mechanical or physical factors, the results suggest that the *in vivo* niche with varied mechanical or physical cues plays an essential role in directing hepatic differentiation of hESCs, together with biochemical inducers.

Author contributions

Chunhua Luo: Investigation, methodology, formal analysis, data curation, writing – original draft, funding acquisition. Dongyuan Lü: Conceptualization, investigation, methodology, formal analysis, data curation, writing – original draft, funding acquisition. Lu Zheng: Investigation. Fan Zhang: Investigation. Xiao Zhang: Investigation. Shouqin Lü: Formal analysis, data curation, funding acquisition. Chen Zhang: Investigation. Xiaohua Jia: Methodology, investigation. Xinyu Shu: Investigation. Peiwen Li: Investigation. Zhan Li: Investigation. Mian Long: Conceptualization, writing – review & editing, supervision, validation, project administration, funding acquisition.

Conflicts of interest

The authors have no conflicts of interest to declare.

Acknowledgements

We thank Dr Ye-Guang Chen from Tsinghua University for providing us H1 hESCs upon Simple Letter of Agreement between Dr Chen's and Dr Long's labs that is approved by the WiCell Research Institute. Drs Lüwen Zhou, Ning Li, and Jin Zhou and Shenbao Chen provided technical assistance in statistical analyses and schematic figure preparations. This work was supported by the National Natural Science Foundation of China grants 91642203, 31627804, 31870931, 31661143044, 31470907, 81703012 and the Chinese Science Academy grants QYZDJ-SSW-JSC018, GJJSTU20190005 and XDB22040101.

References

1 F. M. Watt and B. L. Hogan, Out of eden: stem cells and their niches, *Science*, 2000, **287**, 1427–1430.
2 D. C. Hay, D. Zhao, J. Fletcher, Z. A. Hewitt, D. McLean, A. Urruticoechea-Uriguen, J. R. Black, C. Elcombe, J. A. Ross, R. Wolf and W. Cui, Efficient differentiation of hepatocytes from human embryonic stem cells exhibiting markers recapitulating liver development *in vivo*, *Stem Cells*, 2008, **26**, 894–902.
3 K. A. D'Amour, A. D. Agulnick, S. Eliazer, O. G. Kelly, E. Kroon and E. E. Baetge, Efficient differentiation of human embryonic stem cells to definitive endoderm, *Nat. Biotechnol.*, 2005, **23**, 1534–1541.
4 N. R. F. Hannan, C. P. Segeritz, T. Touboul and L. Vallier, Production of hepatocyte-like cells from human pluripotent stem cells, *Nat. Protoc.*, 2013, **8**, 430–437.
5 D. C. Hay, J. Fletcher, C. Payne, J. D. Terrace, R. C. J. Gallagher, J. Snoeys, J. R. Black, D. Wojtacha, K. Samuel, Z. Hannoun, A. Pryde, C. Filippi, I. S. Currie, S. J. Forbes, J. A. Ross, P. N. Newsome and J. P. Iredale, Highly efficient differentiation of hESCs to functional hepatic endoderm requires ActivinA and Wnt3a signaling, *Proc. Natl. Acad. Sci. U. S. A.*, 2008, **105**, 12301–12306.
6 T. Touboul, N. R. Hannan, S. Corbineau, A. Martinez, C. Martinet, S. Branchereau, S. Mainot, H. Strick-Marchand, R. Pedersen, J. Di Santo, A. Weber and L. Vallier, Generation of functional hepatocytes from human embryonic stem cells under chemically defined conditions that recapitulate liver development, *Hepatology*, 2010, **51**, 1754–1765.
7 H. Baharvand, S. M. Hashemi, S. K. Ashtian and A. Farrokhi, Differentiation of human embryonic stem cells into hepatocytes in 2D and 3D culture systems *in vitro*, *Int. J. Dev. Biol.*, 2006, **50**, 645–652.
8 S. Nonaka, Y. Tanaka, Y. Okada, S. Takeda, A. Harada, Y. Kanai, M. Kido and N. Hirokawa, Randomization of left-right asymmetry due to loss of nodal cilia generating leftward flow of extraembryonic fluid in mice lacking KIF3B motor protein, *Cell*, 1998, **95**, 829–837.
9 N. Motosugi, T. Bauer, Z. Polanski, D. Solter and T. Hiiragi, Polarity of the mouse embryo is established at blastocyst and is not prepatterned, *Genes Dev.*, 2005, **19**, 1081–1092.
10 R. J. Cole, Cinemicrographic observations on the trophoblast and zona pellucida of the mouse blastocyst, *J. Embryol. Exp. Morphol.*, 1967, **17**, 481–490.
11 T. Brunet, A. Bouclet, P. Ahmadi, D. Mitrossilis, B. Driquez, A. C. Brunet, L. Henry, F. Serman, G. Bealle, C. Menager, F. Dumas-Bouchiat, D. Givord, C. Yanicostas, D. Le-Roy, N. M. Dempsey, A. Plessis and E. Farge, Evolutionary conservation of early mesoderm specification by mechanotransduction in Bilateria, *Nat. Commun.*, 2013, **4**, 2821.
12 J. Zoldan, E. D. Karagiannis, C. Y. Lee, D. G. Anderson, R. Langer and S. Levenberg, The influence of scaffold elasticity on germ layer specification of human embryonic stem cells, *Biomaterials*, 2011, **32**, 9612–9621.
13 D. Y. Lü, C. H. Luo, C. Zhang, Z. Li and M. Long, Differential regulation of morphology and stemness of mouse embryonic stem cells by substrate stiffness and topography, *Biomaterials*, 2014, **35**, 3945–3955.
14 A. Cooper, M. Leung and M. Q. Zhang, Polymeric fibrous matrices for substrate-mediated human embryonic stem cell lineage differentiation, *Macromol. Biosci.*, 2012, **12**, 882–892.
15 Y. Du, N. Li, H. Yang, C. H. Luo, Y. X. Gong, C. F. Tong, Y. X. Gao, S. Q. Lu and M. Long, Mimicking liver sinusoidal structures and functions using a 3D-configured microfluidic chip, *Lab Chip*, 2017, **17**, 782–794.
16 J. R. Hu, S. Q. Lü, S. L. Feng and M. Long, Flow dynamics analyses of pathophysiological liver lobules using porous media theory, *Acta Mech. Sin.*, 2017, **33**, 1–10.
17 G. C. Farrell, N. C. Teoh and R. S. McCuskey, Hepatic microcirculation in fatty liver disease, *Anat. Rec.*, 2008, **291**, 684–692.
18 M. Klaas, T. Kangur, J. Viil, K. Maemets-Allas, A. Minajeva, K. Vadi, M. Antsov, N. Lapidus, M. Jarvekulg and V. Jaks, The alterations in the extracellular matrix composition guide the repair of damaged liver tissue, *Sci. Rep.*, 2016, **6**, 27398.
19 Z. Li, Y. W. Gong, S. J. Sun, Y. Du, D. Y. Lü, X. F. Liu and M. Long, Differential regulation of stiffness, topography, and dimension of substrates in rat mesenchymal stem cells, *Biomaterials*, 2013, **34**, 7616–7625.
20 B. Trappmann, J. E. Gautrot, J. T. Connelly, D. G. T. Strange, Y. Li, M. L. Oyen, M. A. C. Stuart, H. Boehm, B. J. Li, V. Vogel, J. P. Spatz, F. M. Watt and W. T. S. Huck, Extracellular-matrix tethering regulates stem-cell fate, *Nat. Mater.*, 2012, **11**, 642–649.
21 H. Deng, W. Shang, G. Lu, P. Guo, T. Ai, C. Fang and J. Tian, Targeted and multifunctional technology for identification between hepatocellular carcinoma and liver cirrhosis, *ACS Appl. Mater. Interfaces*, 2019, **11**, 14526–14537.
22 L. Zheng, D. Y. Lü, F. Zhang, M. Xing, X. Y. Wang, X. H. Jia, X. Y. Shu, P. W. Li, S. Q. Lü, J. Chang and M. Long, Regulation of hepatic differentiation of human embryonic stem cells by calcium silicate extracts for liver injury repairing, *Appl. Mater. Today*, 2020, **20**, 100730.
23 A. Haque, B. Hexig, Q. Meng, S. Hossain, M. Nagaoka and T. Akaike, The effect of recombinant E-cadherin substratum on the differentiation of endoderm-derived hepato-

cyte-like cells from embryonic stem cells, *Biomaterials*, 2011, **32**, 2032–2042.
24 M. Tamai, E. Adachi and Y. Tagawa, Characterization of a liver organoid tissue composed of hepatocytes and fibroblasts in dense collagen fibrils, *Tissue Eng., Part A*, 2013, **19**, 2527–2535.
25 A. J. Engler, S. Sen, H. L. Sweeney and D. E. Discher, Matrix elasticity directs stem cell lineage specification, *Cell*, 2006, **126**, 677–689.
26 N. Mittal, F. Tasnim, C. Yue, Y. H. Qu, D. Phan, Y. Choudhury, M. H. Tan and H. Yu, Substrate stiffness modulates the maturation of human pluripotent stem-cell-derived hepatocytes, *ACS Biomater. Sci. Eng.*, 2016, **2**, 1649–1657.
27 P. Y. Wang, S. Ding, H. Sumer, R. C. Wong and P. Kingshott, Heterogeneity of mesenchymal and pluripotent stem cell populations grown on nanogrooves and nanopillars, *J. Mater. Chem. B*, 2017, **5**, 7927–7938.
28 F. Chowdhury, S. Na, D. Li, Y. C. Poh, T. S. Tanaka, F. Wang and N. Wang, Material properties of the cell dictate stress-induced spreading and differentiation in embryonic stem cells, *Nat. Mater.*, 2010, **9**, 82–88.
29 D. A. Shafritz and M. D. Dabeva, Liver stem cells and model systems for liver repopulation, *J. Hepatol.*, 2002, **36**, 552–564.
30 R. K. Das and O. F. Zouani, A review of the effects of the cell environment physicochemical nanoarchitecture on stem cell commitment, *Biomaterials*, 2014, **35**, 5278–5293.
31 F. Chowdhury, Y. Z. Li, Y. C. Poh, T. Yokohama-Tamaki, N. Wang and T. S. Tanaka, Soft substrates promote homogeneous self-renewal of embryonic stem cells *via* downregulating cell-matrix tractions, *PLoS One*, 2010, **5**, e15655.
32 Y. B. Sun, L. G. Villa-Diaz, R. H. W. Lam, W. Q. Chen, P. H. Krebsbach and J. P. Fu, Mechanics regulates fate decisions of human embryonic stem cells, *PLoS One*, 2012, **7**, e37178.
33 N. D. Evans, C. Minelli, E. Gentleman, V. LaPointe, S. N. Patankar, M. Kallivretaki, X. Y. Chen, C. J. Roberts and M. M. Stevens, Substrate stiffness affects early differentiation events in embryonic stem cells, *Eur. Cells Mater.*, 2009, **18**, 1–13.
34 P. C. Dingal, A. M. Bradshaw, S. Cho, M. Raab, A. Buxboim, J. Swift and D. E. Discher, Fractal heterogeneity in minimal matrix models of scars modulates stiff-niche stem-cell responses *via* nuclear exit of a mechanorepressor, *Nat. Mater.*, 2015, **14**, 951–960.
35 N. A. Lockwood, J. C. Mohr, L. Ji, C. J. Murphy, S. R. Palecek, J. J. de Pablo and N. L. Abbott, Thermotropic liquid crystals as substrates for imaging the reorganization of matrigel by human embryonic stem cells, *Adv. Funct. Mater.*, 2006, **16**, 618–624.
36 S. Gerecht, C. J. Bettinger, Z. Zhang, J. T. Borenstein, G. Vuniak-Novakovic and R. Langer, The effect of actin disrupting agents on contact guidance of human embryonic stem cells, *Biomaterials*, 2007, **28**, 4068–4077.
37 R. Peerani, B. M. Rao, C. Bauwens, T. Yin, G. A. Wood, A. Nagy, E. Kumacheva and P. W. Zandstra, Niche-mediated control of human embryonic stem cell self-renewal and differentiation, *EMBO J.*, 2007, **26**, 4744–4755.
38 R. H. Xu, X. Chen, D. S. Li, R. Li, G. C. Addicks, C. Glennon, T. P. Zwaka and J. A. Thomson, BMP4 initiates human embryonic stem cell differentiation to trophoblast, *Nat. Biotechnol.*, 2002, **20**, 1261–1264.
39 A. Higuchi, Q. D. Ling, S. S. Kumar, Y. Chang, A. A. Alarfaj, M. A. Munusamy, K. Murugan, S. T. Hsu and A. Umezawa, Physical cues of cell culture materials lead the direction of differentiation lineages of pluripotent stem cells, *J. Mater. Chem. B*, 2015, **3**, 8032–8058.
40 T. S. Ramasamy, J. S. Yu, C. Selden, H. Hodgson and W. Cui, Application of three-dimensional culture conditions to human embryonic stem cell-derived definitive endoderm cells enhances hepatocyte differentiation and functionality, *Tissue Eng., Part A*, 2013, **19**, 360–367.
41 S. Snykers, J. De Kock, V. Rogiers and T. Vanhaecke, *In Vitro* Differentiation of Embryonic and Adult Stem Cells into Hepatocytes: State of the Art, *Stem Cells*, 2009, **27**, 577–605.
42 S. Cascio and K. S. Zaret, Hepatocyte differentiation initiates during endodermal-mesenchymal interactions prior to liver formation, *Development*, 1991, **113**, 217–225.
43 H. Basma, A. Soto-Gutierrez, G. R. Yannam, L. Liu, R. Ito, T. Yamamoto, E. Ellis, S. D. Carson, S. Sato, Y. Chen, D. Muirhead, N. Navarro-Alvarez, R. J. Wong, J. Roy-Chowdhury, J. L. Platt, D. F. Mercer, J. D. Miller, S. C. Strom, N. Kobayashi and I. J. Fox, Differentiation and transplantation of human embryonic stem cell-derived hepatocytes, *Gastroenterology*, 2009, **136**, 990–999.
44 P. Huang, Z. He, S. Ji, H. Sun, D. Xiang, C. Liu, Y. Hu, X. Wang and L. Hui, Induction of functional hepatocyte-like cells from mouse fibroblasts by defined factors, *Nature*, 2011, **475**, 386–389.
45 J. A. Heslop and S. A. Duncan, The use of human pluripotent stem cells for modeling liver development and disease, *Hepatology*, 2019, **69**, 1306–1316.
46 J. You, S. A. Park, D. S. Shin, D. Patel, V. K. Raghunathan, M. Kim, C. J. Murphy, G. Tae and A. Revzin, Characterizing the effects of heparin gel stiffness on function of primary hepatocytes, *Tissue Eng., Part A*, 2013, **19**, 2655–2663.
47 J. Fung, C. K. Lee, M. Chan, W. K. Seto, D. K. H. Wong, C. L. Lai and M. F. Yuen, Defining normal liver stiffness range in a normal healthy Chinese population without liver disease, *PLoS One*, 2013, **8**, e85067.
48 U. Arena, F. Vizzutti, G. Corti, S. Ambu, C. Stasi, S. Bresci, S. Moscarella, V. Boddi, A. Petrarca, G. Laffi, F. Marra and M. Pinzani, Acute viral hepatitis increases liver stiffness values measured by transient elastography, *Hepatology*, 2008, **47**, 380–384.
49 C. S. Ranucci, A. Kumar, S. P. Batra and P. V. Moghe, Control of hepatocyte function on collagen foams: sizing matrix pores toward selective induction of 2-D and 3-D cellular morphogenesis, *Biomaterials*, 2000, **21**, 783–793.
50 E. Jain, A. Damania and A. Kumar, Biomaterials for liver tissue engineering, *Hepatol. Int.*, 2014, **8**, 185–197.